HHS Public Access

Author manuscript

Eur J Med Chem. Author manuscript; available in PMC 2015 April 09.

Published in final edited form as:

Eur J Med Chem. 2014 April 9; 76: 506–516. doi:10.1016/j.ejmech.2014.02.046.

Identification of human presequence protease (hPreP) agonists for the treatment of Alzheimer's disease

Jhansi Rani Vangavaragu, **Koteswara Rao Valasani**, **Xueqi Gan**, and **Shirley ShiDu Yan**

Department of Pharmacology and Toxicology, and Higuchi Bioscience Center, School of Pharmacy, University of Kansas, Lawrence, KS 66047, USA

Abstract

Amyloid-β (Aβ), a neurotoxic peptide, is linked to the onset of Alzheimer's disease (AD). Increased Aβ content within neuronal cell mitochondria is a pathological feature in both human and mouse models with AD. This accumulation of Aβ within the mitochondrial landscape perpetuates increased free radical production and activation of the apoptotic pathway. Human Presequence Protease (hPreP) is responsible for the degradation of mitochondrial amyloid-β peptide in human neuronal cells, and is thus an attractive target to increase the proteolysis of Aβ. Therefore, it offers a potential target for Alzheimer's drug design, by identifying potential activators of hPreP. We applied structure-based drug design, combined with experimental methodologies to investigate the ability of various compounds to enhance hPreP proteolytic activity. Compounds **3c** & **4c** enhanced hPreP-mediated proteolysis of Aβ (1–42), $pF_1β$ (2–54) and fluorogenic-substrate V. These results suggest that activation of hPreP by small benzimidazole derivatives provide a promising avenue for AD treatment.

Keywords

Amyloid beta; Alzheimer's disease; enzyme activators; benzimidazole derivatives; hPreP

1. Introduction

Mitochondrial dysfunction is an early pathologic feature of Alzheimer's disease (AD). AD-affected brain shows abnormalities in mitochondrial structure and function including hypometabolism, increased production of reactive oxygen species (ROS) and decreased respiration potential [1–8]. Amyloid-β (Aβ) is a major component of amyloid pathology contributing to the pathogenesis of AD. Recent studies from our and other independent groups demonstrate accumulation of Aβ in mitochondria in aged and AD brain [6, 9–17]. Aβ enters mitochondria through the protein translocase of the outer membrane (TOM) machinery [15]. The receptor for advanced glycation end product (RAGE) also aids in

Corresponding author: Dr. Shirley ShiDu Yan, Departments of Pharmacology and Toxicology and Higuchi Bioscience Center, School of Pharmacy, University of Kansas, 2099 Constant Ave., Lawrence, KS 66047, USA, shidu@ku.edu, Tel: 1-785-864-3637.

localization and transport of mitochondrial Aβ. Neurons lacking RAGE exhibit lowered mitochondrial Aβ accumulation and are protected from Aβ-induced mitochondrial dysfunction [11]. The degree of mitochondrial Aβ accumulation correlates to mitochondrial and synaptic dysfunction as well as cognitive decline observed in AD mouse models. Excess Aβ disrupts normal mitochondrial function thereby inducing oxidative stress, lowered ATP content, and a rise in intercellular Ca^{2+} [14, 16, 18, 19] [20]concentration. Subsequently, an increase in mitochondrial Aβ intensifies its interaction with mitochondrial protein including amyloid binding alcohol dehydrogenase (ABAD)[14, 21] and cyclophilin-D (CypD)[16, 22], exaggerating mitochondrial and neuronal stress. Thus, mitochondria provide a direct site for Aβ-induced mitochondrial damage and reducing Aβ accumulation or increasing Aβ clearance in mitochondria may be a therapeutic strategy for prevention and treatment of AD in particular during early stage.

Human Presequence protease (hPreP), a 114kDa human zinc metalloprotease 1, (hMP1), [23] is located in the mitochondrial matrix [24] and belongs to the pitrilysin M16C family of peptidases containing an inverted zinc-binding motif, HXXEH [25]. hPreP is an ATP-independent protease that consists of 1,037 amino acids (AAH05025) and is encoded by the PITRM1 gene located on chromosome 10 [23]. The presence of human PreP (hPreP) in mitochondrial matrix is confirmed by proteomics 17.31% amino acid sequence [28] and is involved in the degradation of small-unstructured peptides. Importantly, hPreP was found to be the novel protease responsible for the degradation of mitochondrial Aβ in the human AD-affected brain [15, 26, 27].

Although it is a functional analogue to insulin degrading enzyme (IDE), unlike IDE, PreP cannot degrade insulin [24, 28]. It does however degrade Aβ, but the degradation of Aβ peptides by recombinant hPreP results in several fragments that are unique only to hPreP. Despite the fact that the three dimensional structures of PreP [29] and IDE [30] are very similar, IDE harbors an exosite in the catalytic chamber, which is hypothesized to unfold small proteins. The corresponding site is absent in PreP, thereby preventing the degradation of small folded proteins. This makes PreP a better candidate than IDE for clear Aβ since it does not degrade the important insulin protein [24, 28]. The available literature suggests that decreased PreP activity in AD-affected human and mouse neuronal mitochondrial matrixes leads to Aβ aggregation followed by apoptotic cell death. Introduction of hPreP allows for the degradation of Aβ and could prove vital to the understanding of AD pathology.

The literature suggests that increased ROS production [31] is an early indicator of AD pathogenesis and that increased ROS negatively impacts the ability of hPreP to degrade Aβ. In a study, using five to twelve month-old mice [24], PreP proteolytic activity is decreased with age and Aβ-rich mitochondria and AD-affected brain, indicating that there may be a link between overall Prep activity, Aβ accumulation, and age.

We built a three dimensional structural homologous model of hPreP based on the 2.1Å crystal structure of AtPreP [28], in which two cysteines are in close proximity to each other allowing for the possible formation of a disulfide bond under oxidizing conditions inhibiting hPreP activity. A recent study demonstrated that hPreP inactivation by H_2O_2 is not due to the formation of a disulfide bridge, but is instead due to the methionine residues that are

readily oxidized to produce methionine sulfoxide ROS. Conserved methionine residues play an important role in protecting proteins from oxidative inactivation by scavenging oxidizing agents and limiting the damage to catalytically essential residues [32]. This data strongly supports the potential of hPreP to act as a target in the development of AD treatments.

The goal of the present study was to develop small molecules that regulate hPreP function to enhance degradation and clearance of mitochondrial small unstructured peptides including Aβ. We utilized structure based virtual screening to identify novel compounds that bind to the hPreP active site, with the goal of enhancing proteolysis to specific substrates.

2. Results and Discussion

2.1. PreP activators design

It is also well known from the literature that benzimidazole derivatives have antioxidant activity. [34–36] It is also possible that our benzimidazole derivatives could potentially reduce ROS levels. A series of compounds were designed and tested to determine their potential use in AD treatment. Each novel compound was subjected to a structure based virtual screening approach to identify their potential to bind with the hPreP active site. The drug like properties of newly designed compounds was predicted by QSAR and molecular docking studies. The QSAR analysis helped to derive highly applicable models that allowed for the modification of novel reactive molecules. Preliminary structure–activity relationship (SAR) studies indicated that benzimadazole moiety is required for the activation of hPreP activity. This is consistent with the benzimadazole derivative described in the first examples of computer-aided exploration into IDE regulators which can be used for the treatment of AD.[33] The newly designed compounds proposed in this study could serve as initiators for lead optimization studies, which could ultimately lead towards the design of compounds for the treatment of Alzheimer's disease.

2.2. Synthesis

We synthesized a series of novel benzimidazole derivatives (**3a–e** & **4a–e**, shown in Scheme 1), with various aromatic aldehydes, 4-nitrobenzene-1,2-diamine (**2**) by mixing with trimethylsilyl chloride (TMSCL, 1mol %) in water (5mL). The reaction mixture was stirred at room temperature for 8–12 h. TMSCl, an extremely efficient catalyst, was used in the preparation of compounds **4a–e**. All reactions were carried out following this general procedure. Compounds **3a–e** were prepared through the reaction of various aromatic aldehydes with 4-nitrobenzene-1,2-diamine in trifluoroethanol (TFE) at room temperature. The chemical structures of the new compounds were confirmed using: IR, ^{1}H NMR, ^{13}C NMR spectral data and HRMS, the data for which are presented in the Experimental Protocols section. We observed characteristic IR absorption readings in regions at: 3475–3371 cm^{-1} and 3342–3330^{-1}, for: N–H [37, 38], O–H [39, 40], respectively. In the ^{1}H NMR spectra of compounds **3a–e** & **4a–e**, the chemical shifts of aromatic hydrogen's on the phenyl ring appeared as doublets in region and multiplets of 6.96–7.92 and 6.75–7.94 respectively [41, 42]. The O–H hydrogen resonated as a broad singlet in region 11.59–10.97. In ^{13}C NMR, we observed chemical shifts for compounds **3a–e** & **4a–e** in expected regions.

2.3. Quantitative structure-activity relationship (QSAR) descriptors

The three dimensional structures of our compounds (**3a–e** & **4a–e**) were constructed using the builder interface of the molecular operating environment (MOE) program and subjected to energy minimization using the Merck molecular Force Field 94x (MMFF94x)[43, 44]. All items were set to default with an RMS gradient of 0.01 kcal/mol and an RMS distance of 0.1 A°. We subjected the resultant models to a systematic conformational search. Using the above conformations, we studied QSAR descriptors, meeting the Lipinski criteria for safe drugs [45, 46]. Our designed compounds have a molecular weight less than 500 Da with exception of compounds **4c**, **4d** and **4e**. Compound **3a** had the lowest molecular weight (361.35 Da), while compound **4c** had the highest molecular weight (702.90 Da). There were less than 5 numbers of hydrogen bond donors and less than 10 hydrogen bond acceptors for all compounds. LogP values were below 5, indicating that all are non-toxic to the host system. Molar refractivity was in-between 40–150, the optimal range. Characterization of remaining descriptors such as surface area, volume, hydration energy, polarizability and energy levels were also encouraging showing suitable feature in binding domains of the targets and inhibitors suggesting the potential safety and efficacy of these targets (Table 1).

2.4. Molecular modeling [47, 48]

Molecular modeling studies has often been proven to be a powerful tool for rationalizing ligand-receptor interactions and for making this information available to virtual screening techniques. The ligand database that was developed from the total set of ten compounds was docked into the specified binding domain of the hPreP receptor. As we know that PreP is present in Arabidopsis thaliana, and is responsible for the degradation of mitochondrial presequences and elimination of chloroplast transit peptides generated after organelle precursor protein import and processing [49–51], we identified hPreP binding sites using the crystal structure of AtPreP (http://www.rcsb.org/pdb, PDB ID: 2FGE), with residues: Asn136, Ala137, Phe138, Thr139, Ala140, Glu205, Try906, Arg900, Gln222. A total of 30 conformations were generated for each ligand-receptor complex and among them, the conformation with least docking score was considered for further analysis. The MOE interaction of all ligand molecules in the binding domain cavity was analyzed. The ligand-receptor complexes were analyzed by both London G free energy approximations and E interaction energies. Compounds **3c** had the best docking score of −8.6 kcal/mole, followed by docking scores for compound **4c** (−8.3 kcal/mole). Interestingly, compound **3c** formed an arene-hydrogen bond with Gly121 (Figure 1). These two ligands had the best docking scores with stable ligand interactions and are composed of primarily non-polar pi-stacking interactions between Phe 123, Phe124, Try906, Try921, with minimal H-bonding and Zn^{+2} coordination (Figure 1).

2.5. Pharmacophore Model: PreP activators 5 Feature Pharmacophore Model[28, 47, 48]

Using the Pharmacophore five-feature model, shown in Figure 3, we selected 4 out of 10 compounds as ‘hit’s, namely compounds **3c**, **3d**, **4c** and **4d**. Compounds **3c** and **4c** exhibited strong binding against hPreP. Based on the number of hits, the predictive capacity of active hits is at least 50% (Figure 2).

2.6. Evaluation of enzymatic activity of hPreP

Compounds with small molecular weights are necessary to boost hPreP activity and provide therapeutic protection against AD. The literature suggests that hPreP degrades mitochondrial targeting peptides that are cleaved off by mitochondrial processing peptidases following import to mitochondria. PreP's critical role in the degradation of mitochondrial Aβ is significant as accumulation of mitochondrial Aβ is directly linked to Aβ-induced mitochondrial toxicity. Further, hPreP also degrades non-Aβ substrates such as $pF_1\beta$, a 53 amino acid long mitochondrial presequence peptide, and substrate V, a 9 amino acid fluorogenic peptide. Even though these peptides have slightly different properties (Aβ peptides are negatively charged, and $pF_1\beta$ are positively charged), hPreP degrades both with similar efficiency. To our knowledge, compound **3c** & **4c** are the first drug-like compounds shown to stimulate hPreP-mediated proteolysis of various substrates.

To study the regulatory effect of our target compounds (**3a–e** & **4a–e)** on the proteolytic activity of hPreP, we selected three substrates of different lengths and properties for use in an *in vitro* degradation assay: 1)Aβ (1–42); 2) the presequence of ATP synthase $F_1\beta$ subunit $pF_1\beta$ (2–54); 3) and a fluorescent peptide known as substrate V. Activity assays were initially set at a concentration of 100 μM for all studied molecules in order to identify the effect of those compounds on overall hPreP activity. We quantified hPreP activity by monitoring the change in fluorescence for proteolysis of fluorogenic-substrate V and monitored the efficacy of degradation of Aβ (1–42) & $pF_1\beta$, using immunoblotting for Aβ with NuPAGE 12% Bis-tris gel assay.

Analysis of compounds showed that **3c** & **4c** increased proteolytic activity of hPreP against biotin labeled Aβ (1–42), significant up to a 1μM concentration when compared to other analogs. Compounds **3c** & **4c** effectively facilitated the degradation of Aβ at more efficient levels than hPreP alone (Figure 3A & 4A). We observed degenerated and dose dependent immunoreactive biotin Aβ bands due to the enhanced proteolytic activity of hPreP at various concentrations of compound **3c** & **4c** (Figure 3C, D & 4C, D), with no Aβ immunoreactive bands at 100μM (Figure 3D & 4D, lane 5), compared to hPreP alone. Analysis for the effect of compounds on hPreP activity showed that **3c** increased the hPreP -mediated Aβ degradation by 1.7 (42%) & **4c** by 2.1 folds (54%) (Figure 9A).

Next, we analyzed an EC50 value of each molecule that enhanced hPreP activity using a dose response assay, where specific activity of hPreP was measured with different concentrations of the lead compounds and then the plot was fit to prism nonlinear regression, a log (agonist) vs. normalized response equation. Calculated EC_{50} values for **3c** & **4c** were 0.713 μM and 0.402 μM, respectively (Figure 3B & 4B).

In the case of non-Aβ substrates, hPreP also degraded $pF_1\beta$ and compounds **3c** & **4c** showed significant proteolytic activity of hPreP in degrading $pF_1\beta$ even at 1μM concentration. Significant changes in $pF_1\beta$ degradation were observed with compounds **3c** & **4c** when compared to hPreP alone (Figure 5A & 6A). In figures 5C & 6C the presence of degenerated & dose dependent immunoreactive biotin $pF_1\beta$ bands, indicate enhanced proteolytic activity of hPreP with different concentrations of compounds **3c** & **4c**. Compounds **3c** & **4c** increased hPreP-mediated $pF_1\beta$ degradation by 1.8 (45%) & 2.2 folds (55%) respectively

(Figure 9B). EC_{50} values for **3c** & **4c** were measured at 0.012 & 0.601μM, respectively (Figure 5B & 6B).

Further, we performed kinetic studies using Substrate V, a fluorogenic peptide 9 amino acids long containing the fluorescent group 7-methoxycoumarin and the quencher group 2, 4-dinitrophenyl, thus, providing light emission upon cleavage of the peptide bond between these two groups. Compounds, **3c** & **4c** increased the initial rate of proteolysis activity of hPreP the most, specifically by 1.5 and 1.8 folds, respectively at 1μM (Figures 7A & 8A). Further, the EC_{50} values for **3c** & **4c** were 0.152 & 0.057 μM, respectively (Figures 7B & 8B).

Interestingly, condensation of 5-bromo-2-hydroxy benzaldehyde with nitro *o*-phenelene diamine plays a crucial role in bioactivity of our compounds **3c** & **4c**. Introduction of a 5-bromo-2-hydroxy group (**3c** into the benzimidazole ring) enhanced the proteolytic activity of hPreP against biotin Aβ (1–42), pF1β (2–54) and substrate V. The same correlation was also observed in compound **4c** against these three aforementioned substrates. It is clear that the presence of a bromo group on the aromatic ring is essential for improving hydrophilic interactions between the compound and hPreP. Substitution of the fluoro, methoxy & hydroxy in the aromatic aldehyde caused a substantial loss of proteolytic activity of hPreP. These results suggest that the compounds with halogen atoms (bromo) that underwent hydroxyl substitution on their phenyl ring(s) (**3c** & **4c**) were the most potent and selective activators for the proteolytic activity of hPreP. Our results clearly indicate that benzimidazole analogues shed new light on the design and understanding of selective proteolytic enzyme activators, which will enable the synthesis of our scaffold into clinically useful anti-Alzheimer's drugs.

3. Conclusion

In the present study, we designed novel benzimidazole derivatives according to their binding modes inside the hPreP active site. Amongst them, we selected compounds that obeyed the Lipinski's "rule of five." This is extensively used to screen for the drug-like properties. Our novel compounds behaved like hPreP agonists, with compounds **3c** & **4c** being most active. Introduction of a 5-bromo-2-hydroxy benzaldehyde group increased potency resulting in the 4-bromo-2-(1-(5-bromo-2-hydroxybenzyl)-5-nitro-1H-benzo[d]imidazol-2-yl) phenol & 2,2′-((2-(5-bromo-2-hydroxyphenyl)-5-nitro-1H-benzo[d]imidazole-1,3(2H) diyl)bis(methylene))bis(4-bromophenol), which are the most active compounds (at 100 μM) and seem to be good agonists of hPreP with EC_{50} in the low μM range.

Together with biological results (indicating that the synthesized benzimidazole-based compounds possess agonist activity with hPreP) and the results of the docking studies and regulating activities, we conclude that compounds **3c** & **4c** are appropriate scaffolds for the development of new hPreP regulators. Further investigation of the effect of these benzimadazole derivatives on hPreP agonist activity will move the development of new agents for the treatment of AD forward towards translation to clinical use.

4. Materials and Methods

4.2. Chemistry

4.2.1. General—All reagents were commercially available and used without further purification. Melting points were determined in open capillary tubes using a Laboratory Devices Mel-Temp apparatus and are uncorrected. ^{1}H and ^{13}C NMR spectra were recorded in d_6-DMSO on a Bruker DRX-500 spectrometer operating at 500 MHz, and 125 MHz, respectively, and calibrated to the solvent peak. Abbreviations used for the split patterns of proton NMR signals are: singlet (s), doublet (d), triplet (t), quartet (q), quintet (qui), multiplet (m) and broad signal (br). High-resolution mass spectrometry (HRMS) was recorded on a LCT Premier Spectrometer.

4.2.2. General procedure for the preparation of compounds (3a–3e)—A mixture of aromatic aldehyde (2 mmol), 4-nitrobenzene-1, 2-diamine (1 mmol, 2 equiv), and TFE (1mL) was stirred magnetically at room temperature for 1h. The progress of the reaction was monitored using TLC (hexane: ethyl acetate, 1:1 v/v). After completion of the reaction, the reaction mixture was dissolved in EtOAc (3 mL), adsorbed on silica gel (0.5 g, 230–400 mesh), and concentrated under rotary vacuum evaporation. The resultant solid mass was charged onto a flash chromatography column and eluted with hexane-EtOAc (85:15) to afford the title compounds.

4.2.3. 4-(1-(4-Hydroxybenzyl)-5-nitro-1H-benzo[d]imidazol-2-yl) phenol (3a)—Light color solid, 77% yield; mp: 185–186 °C; R_f 0.22; (hexane: ethyl acetate, 1:1 v/v). IR: 3234, 3050, 2902, 2864, 2362, 1712, 1668, 1529, 1431, 1350, 1257, 1091, 1031, 748 $cm^{-1;}$ ^{1}H NMR (DMSO-d_6) ™ 10.15 (s, 1H), 9.46 (s, 1H), 8.45 (d, J = 3.75 Hz, 1H), 8.15-8.13 (m, 1H) 7.84 (d, J = 3.75 Hz, 1H), 7.67-7.63 (m, 2H), 6.94-6.91 (m, 2H), 6.69-6.66 (m, 2H), 5.61 (s, 2H). ^{13}C NMR (DMSO-d_6)™ 159.6, 158.6, 156.8, 147.6, 142.6, 135.4, 130.9, 127.5, 126.4, 119.6, 119.0, 117.8, 115.7 (J = 15.0 Hz), 47.6. HRMS cald for $C_{20}H_{16}N_3O_{54}$ (M+H) 362.1132; found 362.1141 (TOF MS ES^+).

4.2.4. 1-(4-Fluorobenzyl)-2-(4-fluorophenyl)-5-nitro-1H-benzo[d]imidazole (3b)—Yellow solid, 88% yield; mp: 201–203 °C; R_f 0.32; (hexane: ethyl acetate, 1:1 v/v). IR: 3076, 3055, 2948, 2765, 1897, 1610, 1523, 1483, 1329, 1265, 1172, 1110, 954, 823, 748 $cm^{-1;}$ ^{1}H NMR (DMSO-d_6)™ 8.63-8.61 (m, 1H), 8.22-8.18 (s, 1H), 7.86-7.79 (m, 3H) 7.45-7.40 (t, 2H), 7.15-7.02 (m, 4H), 5.76-5.68 (m, 2H). ^{13}C NMR (DMSO-d_6) ™ 164.3(d, J = 7.5 Hz), 162.4, 160.4(d, J = 3.75 Hz), 157.2, 156.1, 146.9, 143.2, 142.9, 141.6, 140.2, 135.3, 132.4(d, J = 3.75 Hz), 132.2(d, J = 2.5 Hz), 131.7, 128.3(d, J = 8.75 Hz), 119.6, 118.4, 118.0, 116.1, 115.9, 115.7, 115.6, 115.4, 111.7, 108.1, 47.2 (d, J = 15 Hz). HRMS cald for $C_{20}H_{14}F_2N_3O_2$ (M+H) 366.1052; found 366.1054 (TOF MS ES^+).

4.2.5. 4-Bromo-2-(1-(5-bromo-2-hydroxybenzyl)-5-nitro-1H-benzo[d]imidazol-2-yl) phenol (3c)—White crystals, 78% yield; mp: 226–228 °C; R_f 0.32; (hexane: ethyl acetate, 1:1 v/v). IR: 3475, 3342, 3055, 2989, 2893, 2304, 1903, 1629, 1610, 1579, 1488, 1434, 1348, 1222, 1176, 977, 896, 748 $cm^{-1;}$ ^{1}H NMR (DMSO-d_6) ™ 11.60 (s, 2H), 8.92 (s, 2H), 8.12 (d, 1H) 7.96-7.93 (m, 2H), 7.56-7.53 (m, 2H), 6.96 (d, J = 10.0 Hz, 2H), 6.81-6.78

(m, 2H). ^{13}C NMR (DMSO-d$_6$) ™ 159.1, 158.3, 150.3, 136.0, 135.5, 133.6, 132.5, 124.4, 122.6, 199.0, 144.1, 113.1, 110.4. HRMS cald for $C_{20}H_{13}Br_2N_3O_4$ (M+H); 517.9351, found 517.9352 (TOF MS ES$^+$).

4.2.6. Methyl 2-hydroxy-5-(1-(4-hydroxy-3-(methoxycarbonyl)benzyl)-5-nitro-1H-benzo[d]imidazol-2-yl)benzoate (3e)—Yellow solid, 86% yield; mp: 265–267 °C; R_f 0.20; (hexane: ethyl acetate, 1:1 v/v). IR: 3371, 3055, 2950, 2767, 1903, 1627, 1612, 1487, 1265, 1176, 977, 896, 817, 738 cm$^{-1;}$ ^{1}H NMR (DMSO-d$_6$) ™ 11.06 (s, 2H), 8.88-8.68(m, 2H), 8.45-8.38 (m, 5H), 8.15-8.13 (m, 1H) 7.78 (d, *J* = 5.0 Hz, 2H), 7.24 (d, *J* = 10.0 Hz, 2H), 3.96 (s, 6H). ^{13}C NMR (DMSO-d$_6$) ™ 167.8, 162.0, 154.0, 143.1, 141.2, 137.1, 133.8, 130.0, 118.7, 118.5, 114.7, 114.4, 111.1, 52.6. HRMS cald for $C_{24}H_{20}N_3O_8$ (M+H) 478.1250; found 478.1259 (TOF MS ES$^+$).

4.2.7. General procedure for the preparation of compounds (4a–4e)—To a stirred solution aromatic aldehyde (3 mmol), 4-nitrobenzene-1, 2-diamine (1 mmol, 2 equiv), was added in the presence of trimethylsilylchloride dissolved in water (5 mL). The reaction mixture was stirred for 8–12 h at room temperature. The progress of the reaction was monitored by TLC (hexane: ethylacetate1:1). After completion of the reaction, a solid was formed. The solid was filtered off, washed with water, and dried. It was purified by silica gel column chromatography eluting with hexane: ethyl acetate (95:5) mixture to afford the title compounds.

4.2.8. 4,4′-((2-(4-Hydroxyphenyl)-5-nitro-1H-benzo[d]imidazole-1,3(2H)-diyl)bis(methylene)) diphenol (4a)—Light orange color solid; mp: 224–226 °C; R_f 0.24; (hexane: ethyl acetate, 1:1 v/v). IR: 3234, 3103, 2902, 2796, 2362, 1712, 1668, 1529, 1350, 1091, 1031, 881, 738 cm$^{-1;}$ ^{1}H NMR (DMSO-d$_6$) δ 10.23 (s, 1H), 9.45 (s, 2H), 8.48 (d, *J* = 3.75 Hz, 2H), 8.15-8.13 (m, 2H) 7.68-7.62 (m, 4H), 7.01–7.06 (m, 3H), 6.82–6.89 (m, 3H), 6.71-6.69 (m, 2H), 5.56 (s, 4H). ^{13}C NMR (DMSO-d$_6$) δ 160.3, 159.2, 158.0, 148.1, 142.8, 136.1, 131.2, 128.6, 127.5, 120.0, 119.4, 118.5, 116.8 (*J* = 15.0 Hz), 48.1. HRMS cald for $C_{27}H_{24}N_3O_5$ (M+H) 470.1716; found 470.1761(TOF MS ES$^+$).

4.2.9. 1,3-Bis(4-fluorobenzyl)-2-(4-fluorophenyl)-5-nitro-2,3-dihydro-1H-benzo[d]imidazole (4b)—Yellow solid, 92% yield; mp: 196–198 °C; R_f 0.30; (hexane: ethyl acetate, 1:1 v/v). IR: 3099, 3055, 2927, 2761, 1895, 1730, 1610, 1579, 1483, 1344, 1265, 1174, 1110, 896, 748 cm$^{-1;}$ ^{1}H NMR (DMSO-d$_6$) δ 8.68-8.59 (m, 2H), 8.28-8.22 (s, 2H), 7.70-7.59 (m, 5H) 7.48-7.41 (m, 4H), 7.16-7.01(m, 4H), 5.80-5.71 (m, 4H). ^{13}C NMR (DMSO-d$_6$) δ 165.2, 163.2, 161.1(d, *J* = 3.75 Hz), 158.1, 158.1, 142.1, 140.5, 139.8, 138.8, 138.2, 136.3, 131.4(d, *J* = 3.75 Hz), 131.1, 129.2, 127.3, 120.6, 119.3, 118.2, 116.8, 115.9, 115.2, 114.2, 113.2, 110.1, 107.1, 48.3 (d, *J* = 15 Hz). HRMS cald for $C_{27}H_{21}F_3N_3O_2$ (M +H) 476.1586; found 476.1591 (TOF MS ES$^+$).

4.2.10. 2,2′-((2-(5-Bromo-2-hydroxyphenyl)-5-nitro-1H-benzo[d]imidazole-1,3(2H) diyl)bis(methylene))bis(4-bromophenol) (4c)—White crystals, 82% yield; mp: 256–257 °C; R_f 0.28; (hexane: ethyl acetate, 1:1 v/v). IR: 3330, 3236, 2927, 2883, 1924, 1714, 1668, 1568, 1525, 1346, 1253, 1091, 1051, 881, 738, 698 cm$^{-1;}$ ^{1}H NMR (DMSO-d$_6$) ™ 11.59 (s, 2H), 8.94 (s, 2H), 8.12 (d, 2H) 7.96-7.94 (m, 4H),

7.56-7.54 (m, 2H), 6.96 (d, *J* = 10.0 Hz, 2H), 6.80-6.78 (m, 6H). ^{13}C NMR (DMSO-d_6) ™ 159.1, 158.3, 150.3, 136.0, 135.5, 133.6, 132.5, 124.4, 122.6, 199.0, 144.1, 113.1, 110.4. HRMS cald for $C_{27}H_{20}Br_3N_3O_5$ (M+H) 702.8953; found 702.8922 (TOF MS ES$^+$).

4.2.11. Dimethyl 5,5′-((2-(4-hydroxy-3-(methoxycarbonyl)phenyl)-5-nitro-1H-benzo[d]imidazole-1,3(2H)-diyl)bis(methylene))bis(2-hydroxybenzoate) (4e)— White crystals, 72% yield; mp: 286–288 °C; R_f 0.18; (hexane: ethyl acetate, 1:1 v/v). IR: 3055, 2989, 2950, 1629, 1579, 1587, 1534, 1487,1222, 1176, 977, 817, 750 cm$^{-1;}$ ^{1}H NMR (DMSO-d_6) ™ 10.97 (s, 3H), 8.81 (d, *J* = 5.0 Hz, 3H), 8.41 (m, 2H), 8.32-8.30 (m, 1H), 8.15-8.13 (m, 1H) 8.00 (d, *J* = 5.0 Hz, 3H), 7.92 (d, *J* = 5.0 Hz, 1H), 7.14-7.11 (m, 3H), 6.77-6.75 (m, 4H), 3.94 (s, 9H). ^{13}C NMR (DMSO-d_6) ™ 168.5, 162.2, 158.6, 150.9, 135.9, 135.0, 134.2, 132.4, 127.8, 124.1, 118.0, 113.8, 113.0, 112.5, 52.6. HRMS cald for $C_{33}H_{30}N_3O_{11}$ (M+H) 644.1880; found 644.1852 (TOF MS ES$^+$).

4.1.1. Preparation of human PreP homology model [28]—A Blast (NCBI, www.ncbi.nih.gov) database search of the PDB Databank revealed the optimal starting template structure for human PreP as a zinc metalloprotease ((PDB:http://www.rcsb.org/pdb, PDB ID: 2FGE). Sequence homology construction of the human PMP1 enzyme sequence based on 2FGE structure was carried out using a MOE protein homology algorithm. Hydrogens were added to the resulting 3D structure based on a pH of 7 and a salt concentration of 0.1 M. pH of 7. The implicit born solvation model and a non-bonded cut off value of 10–12 were incorporated in the MMFF94x force field. The complete structure was energy minimized to a gradient cut off value of 0.05. Molecular dynamic simulations were carried out at a constant temperature of 300° K for a heating time of 10 pico seconds. Simulations were carried out for 10 nano seconds. The time step was considered as 0.001 pico seconds and the temperature relaxation time was set to 0.2 pico seconds. Position, velocity and acceleration were saved every 0.5 pico seconds.

4.1.2. Prediction of Binding site for Ligands—The binding site of hPreP was elucidated through the crystal structure of AtPreP (PDB:http://www.rcsb.org/pdb, PDB ID: 2FGE). In our case, we used a proximity radius of r </= 10 A^o. A confirmatory approach for determining the binding site of these novel drug-like candidates involved use of Alpha Site Finder methodology [Edelsbrunner, *et al*. “Measuring Proteins and Voids in Proteins”,. Proceedings from the 28th International Conference on Systems Science, 256–264(1995)], incorporated into the Chemical Computing Group’s the molecular modeling software. This algorithm calculates and displays potential regions of tight atomic packing on a protein surface.

4.1.3. Molecular Docking [24, 25]—A conformational set was generated for each of our ligand molecules using the *LowModeMD Search* algorithm within the MOE program. This involves a short molecular dynamics simulation using velocities with low kinetic energy on high-frequency vibrational modes. An iteration limit of 5000 (maximum number of attempts to generate a new conformation) and a minimization limit of 250 (maximum number of minimization steps) were set to control the number of conformations generated. Each generated conformation was docked into the specified binding domain of the human PreP

receptor. We analyzed interaction of all ligand molecules in the binding domain cavity using ligand interaction study in the MOE software. The ligand-receptor complexes were analyzed using the sum of the following two scoring functions: (*i)* London ⊗G free energy approximations and (*ii)* interaction energies, ⊗E. Ligands that bound with the lowest docking score were considered for further analysis.

4.1.4. Pharmacophore Model—A pharmacophore defines features as well as locations of important binding interactions between a ligand and its receptor. Our five-feature pharmacophore model was constructed by overlapping the top two ligand candidates (compounds **3c** and **4c**) that had the strongest binding affinities. The Unified scheme within MOE was used to define the unique features (2 H-bond [Don/Acc] and 3 aromatic centers [Aro]). The locations of these features were determined by inspection of strong interactions of these two compounds at the PreP active site.

4.3. Degradation assays

For the analysis of the novel compounds as chemical regulators for hPreP activity, we performed degradation assays with biotin-labeled Aβ (1–42) and F_1β (2–54) [36] presequence peptides in degradation buffer (20mM HEPES-KOH pH 8.0) with10mM MgCl2, 1μg of purified hPreP and 0.02μg of a substrate at various concentrations (0.00001–100μM). Compounds were incubated for 2.5 h at 37^3C. Reactions were stopped by the addition of 4× sample buffer, and then analyzed on NuPAGE 12% Bis-Tris gel (Invitrogen, CA), and run in 1×MES buffer. Proteins were electrophoretically transferred to nitrocellulose membrane HybondTM (Amersham Bioscience) for 1 h at 100V. For pF1β identification, the nitrocellulose membrane was blocked overnight in 5% milk-PBS followed by incubation with pF1β antibody (1:2000) and detected using horseradish peroxidase-conjugated anti-rabbit secondary antibody (1:2500) and enhanced chemiluminescence (ECL, GE Healthcare). For analyzing the degradation of biotin labeled Aβ (1–42) (biotin- LC-Aβ1–40, biotin-LC- Aβ1–42), the nitrocellulose membrane was dried overnight at 25^3C followed by blocking with 2% milk-PBS for 1 h. Immunoblotting was performed with ExtraAvidin Peroxidase Conjugate 1:3000 (Sigma) and detection by ECL.

4.4. Degradation of Substrate V by hPrep

To determine the efficiency of these novel compounds as chemical regulators for hPreP activity, we used a fluorescence assay with fluorogenic substrate V (7-methoxycoumarin-4-yl-acetyl-NPPGFSAFK-2, 4-dinitrophenyl, R&D Systems) and measured the kinetics of proteolysis. Reaction was carried out in the presence of 1μg hPreP in 20mM HEPES, pH 8.0 with 10mM $MgCl_2$ mixed with 0.1μg Substrate V and various concentrations (0.00001–1μM) of our compounds in a final volume of 250μl. The hydrolysis of substrate V was measured for 10 minutes using a fluorometer (SpectraMax Gemini) with excitation and emission wavelengths set at 320 and 405 nm, respectively. Results are shown as the Substrate V degradation rate and averaged over three independent experiments (Figure 7)

4.5. Statistical analysis

Statistical analyses were performed using STATVIEW software. One-way ANOVA was used for repeated measures followed by Bonferroni/Dunn Protected Least Significant

Difference analysis for post-hoc comparisons. Results are expressed as mean ± Standard Error Mean (SEM). Significance was set at $p < 0.05$.

Supplementary Material

Refer to Web version on PubMed Central for supplementary material.

Acknowledgments

This study was supported by grant awards (R01GM095355, R37AG037319, and RO1NS65482) from the National Institute of General Medical Sciences, the National Institute on Aging, and the National Institute of Neurological Disease and Stroke.

References

1. Maurer I, Zierz S, Moller HJ. A selective defect of cytochrome c oxidase is present in brain of Alzheimer disease patients. Neurobiology of aging. 2000; 21:455–462. [PubMed: 10858595]
2. Sheehan JP, Swerdlow RH, Miller SW, Davis RE, Parks JK, Parker WD, Tuttle JB. Calcium homeostasis and reactive oxygen species production in cells transformed by mitochondria from individuals with sporadic Alzheimer's disease. The Journal of neuroscience : the official journal of the Society for Neuroscience. 1997; 17:4612–4622. [PubMed: 9169522]
3. Swerdlow RH, Khan SM. A "mitochondrial cascade hypothesis" for sporadic Alzheimer's disease. Medical hypotheses. 2004; 63:8–20. [PubMed: 15193340]
4. Du H, Yan SS. Mitochondrial medicine for neurodegenerative diseases. The international journal of biochemistry & cell biology. 2010; 42:560–572. [PubMed: 20067840]
5. Lin MT, Beal MF. Alzheimer's APP mangles mitochondria. Nature medicine. 2006; 12:1241–1243.
6. Eckert A, Hauptmann S, Scherping I, Rhein V, Muller-Spahn F, Gotz J, Muller WE. Soluble beta-amyloid leads to mitochondrial defects in amyloid precursor protein and tau transgenic mice. Neuro-degenerative diseases. 2008; 5:157–159. [PubMed: 18322377]
7. Yao J, Irwin RW, Zhao L, Nilsen J, Hamilton RT, Brinton RD. Mitochondrial bioenergetic deficit precedes Alzheimer's pathology in female mouse model of Alzheimer's disease. Proceedings of the National Academy of Sciences of the United States of America. 2009; 106:14670–14675. [PubMed: 19667196]
8. Caspersen C, Wang N, Yao J, Sosunov A, Chen X, Lustbader JW, Xu HW, Stern D, McKhann G, Yan SD. Mitochondrial Abeta: a potential focal point for neuronal metabolic dysfunction in Alzheimer's disease. The FASEB journal : official publication of the Federation of American Societies for Experimental Biology. 2005; 19:2040–2041.
9. Yao J, Irwin RW, Zhao L, Nilsen J, Hamilton RT, Brinton RD. Mitochondrial bioenergetic deficit precedes Alzheimer's pathology in female mouse model of Alzheimer's disease. Proc Natl Acad Sci U S A. 2009
10. Yao J, Du H, Yan S, Fang F, Wang C, Lue LF, Guo L, Chen D, Stern DM, Gunn Moore FJ, Xi Chen J, Arancio O, Yan SS. Inhibition of amyloid-beta (Abeta) peptide-binding alcohol dehydrogenase-Abeta interaction reduces Abeta accumulation and improves mitochondrial function in a mouse model of Alzheimer's disease. J Neurosci. 2011; 31:2313–2320. [PubMed: 21307267]
11. Takuma K, Fang F, Zhang W, Yan S, Fukuzaki E, Du H, Sosunov A, McKhann G, Funatsu Y, Nakamichi N, Nagai T, Mizoguchi H, Ibi D, Hori O, Ogawa S, Stern DM, Yamada K, Yan SS. RAGE-mediated signaling contributes to intraneuronal transport of amyloid-beta and neuronal dysfunction. Proceedings of the National Academy of Sciences of the United States of America. 2009; 106:20021–20026. [PubMed: 19901339]
12. Pavlov PF, Petersen CH, Glaser E, Ankarcrona M. Mitochondrial accumulation of APP and Abeta: Significance for Alzheimer disease pathogenesis. J Cell Mol Med. 2009
13. Manczak M, Anekonda TS, Henson E, Park BS, Quinn J, Reddy PH. Mitochondria are a direct site of A beta accumulation in Alzheimer's disease neurons: implications for free radical generation

and oxidative damage in disease progression. Hum Mol Genet. 2006; 15:1437–1449. [PubMed: 16551656]

14. Lustbader JW, Cirilli M, Lin C, Xu HW, Takuma K, Wang N, Caspersen C, Chen X, Pollak S, Chaney M, Trinchese F, Liu S, Gunn-Moore F, Lue LF, Walker DG, Kuppusamy P, Zewier ZL, Arancio O, Stern D, Yan SS, Wu H. ABAD directly links Abeta to mitochondrial toxicity in Alzheimer's disease. Science. 2004; 304:448–452. [PubMed: 15087549]
15. Hansson Petersen CA, Alikhani N, Behbahani H, Wiehager B, Pavlov PF, Alafuzoff I, Leinonen V, Ito A, Winblad B, Glaser E, Ankarcrona M. The amyloid beta-peptide is imported into mitochondria via the TOM import machinery and localized to mitochondrial cristae. Proc Natl Acad Sci U S A. 2008; 105:13145–13150. [PubMed: 18757748]
16. Du H, Guo L, Fang F, Chen D, Sosunov AA, McKhann GM, Yan Y, Wang C, Zhang H, Molkentin JD, Gunn-Moore FJ, Vonsattel JP, Arancio O, Chen JX, Yan SD. Cyclophilin D deficiency attenuates mitochondrial and neuronal perturbation and ameliorates learning and memory in Alzheimer's disease. Nat Med. 2008; 14:1097–1105. [PubMed: 18806802]
17. Dragicevic N, Mamcarz M, Zhu Y, Buzzeo R, Tan J, Arendash GW, Bradshaw PC. Mitochondrial amyloid-beta levels are associated with the extent of mitochondrial dysfunction in different brain regions and the degree of cognitive impairment in Alzheimer's transgenic mice. J Alzheimers Dis. 2010; 20(Suppl 2):S535–550. [PubMed: 20463404]
18. Butterfield DA, Hensley K, Harris M, Mattson M, Carney J. beta-Amyloid peptide free radical fragments initiate synaptosomal lipoperoxidation in a sequence-specific fashion: implications to Alzheimer's disease. Biochemical and biophysical research communications. 1994; 200:710–715. [PubMed: 8179604]
19. Cardoso SM, Santana I, Swerdlow RH, Oliveira CR. Mitochondria dysfunction of Alzheimer's disease cybrids enhances Abeta toxicity. Journal of neurochemistry. 2004; 89:1417–1426. [PubMed: 15189344]
20. Cakir B, Dagliyan O, Dagyildiz E, Baris I, Kavakli IH, Kizilel S, Turkay M. Structure based discovery of small molecules to regulate the activity of human insulin degrading enzyme. Plos One. 2012; 7:e31787. [PubMed: 22355395]
21. Takuma K, Yao J, Huang J, Xu H, Chen X, Luddy J, Trillat AC, Stern DM, Arancio O, Yan SS. ABAD enhances Abeta-induced cell stress via mitochondrial dysfunction. Faseb J. 2005; 19:597–598. [PubMed: 15665036]
22. Du H, Guo L, Zhang W, Rydzewska M, Yan S. Cyclophilin D deficiency improves mitochondrial function and learning/memory in aging Alzheimer disease mouse model. Neurobiology of aging. 2011; 32:398–406. [PubMed: 19362755]
23. Mzhavia N, Berman YL, Qian Y, Yan L, Devi LA. Cloning, expression, and characterization of human metalloprotease 1: a novel member of the pitrilysin family of metalloendoproteases. DNA and cell biology. 1999; 18:369–380. [PubMed: 10360838]
24. Falkevall A, Alikhani N, Bhushan S, Pavlov PF, Busch K, Johnson KA, Eneqvist T, Tjernberg L, Ankarcrona M, Glaser E. Degradation of the amyloid beta-protein by the novel mitochondrial peptidasome, PreP. J Biol Chem. 2006; 281:29096–29104. [PubMed: 16849325]
25. Becker AB, Roth RA. An unusual active site identified in a family of zinc metalloendopeptidases. Proceedings of the National Academy of Sciences of the United States of America. 1992; 89:3835–3839. [PubMed: 1570301]
26. Taylor SW, Fahy E, Zhang B, Glenn GM, Warnock DE, Wiley S, Murphy AN, Gaucher SP, Capaldi RA, Gibson BW, Ghosh SS. Characterization of the human heart mitochondrial proteome. Nature biotechnology. 2003; 21:281–286.
27. Alikhani N, Ankarcrona M, Glaser E. Mitochondria and Alzheimer's disease: amyloid-beta peptide uptake and degradation by the presequence protease, hPreP. Journal of bioenergetics and biomembranes. 2009; 41:447–451. [PubMed: 19798557]
28. Johnson KA, Bhushan S, Stahl A, Hallberg BM, Frohn A, Glaser E, Eneqvist T. The closed structure of presequence protease PreP forms a unique 10,000 Angstroms3 chamber for proteolysis. The EMBO journal. 2006; 25:1977–1986. [PubMed: 16601675]
29. Maduke M, Roise D. Import of a mitochondrial presequence into protein-free phospholipid vesicles. Science. 1993; 260:364–367. [PubMed: 8385804]

30. Shen Y, Joachimiak A, Rosner MR, Tang WJ. Structures of human insulin-degrading enzyme reveal a new substrate recognition mechanism. Nature. 2006; 443:870–874. [PubMed: 17051221]
31. Butterfield DA. Amyloid beta-peptide (1–42)-induced oxidative stress and neurotoxicity: implications for neurodegeneration in Alzheimer's disease brain. A review. Free radical research. 2002; 36:1307–1313. [PubMed: 12607822]
32. Teixeira PF, Pinho CM, Branca RM, Lehtio J, Levine RL, Glaser E. In vitro oxidative inactivation of human presequence protease (hPreP). Free radical biology & medicine. 2012; 53:2188–2195. [PubMed: 23041349]
33. Cakir B, Dagliyan O, Dagyildiz E, Baris I, Kavakli IH, Kizilel S, Turkay M. Structure Based Discovery of Small Molecules to Regulate the Activity of Human Insulin Degrading Enzyme. Plos One. 2012; 7
34. Nile SH, Kumar B, Park SW. In Vitro Evaluation of Selected Benzimidazole Derivatives as an Antioxidant and Xanthine Oxidase Inhibitors. Chemical biology & drug design. 2013; 82:290–295. [PubMed: 23581708]
35. Ayhan-Kilcigil G, Kus C, Ozdamar ED, Can-Eke B, Iscan M. Synthesis and antioxidant capacities of some new benzimidazole derivatives. Arch Pharm. 2007; 340:607–611.
36. Gurer-Orhan H, Orhan H, Suzen S, Puskullu MO, Buyukbingol E. Synthesis and evaluation of in vitro antioxidant capacities of some benzimidazole derivatives. J Enzym Inhib Med Ch. 2006; 21:241–247.
37. Koteswara Rao V, Janardhan Rao A, Subba Reddy S, Naga Raju C, Visweswara Rao P, Ghosh SK. Synthesis, spectral characterization and biological evaluation of phosphorylated derivatives of galanthamine. European journal of medicinal chemistry. 2010; 45:203–209. [PubMed: 19853328]
38. Rao VK, Reddy SS, Krishna BS, Reddy CS, Reddy NP, Reddy TCM, Raju CN, Ghosh SK. Design, Synthesis and Anti Colon Cancer Activity Evaluation of Phosphorylated Derivatives of Lamivudine (3TC). Lett Drug Des Discov. 2011; 8:59–64.
39. Jhansi Rani V, Raghavendra A, Kishore P, Nanda Kumar Y, Hema Kumar K, Jagadeeswarareddy K. Synthesis and biological activity evaluation of cytidine-5′-deoxy-5-fluoro-N-[(alkoxy/aryloxy)] carbonyl-cyclic 2′,3′-carbonates. European journal of medicinal chemistry. 2012; 54:690–696. [PubMed: 22796042]
40. Rani VJ, Aminedi R, Polireddy K, Jagadeeswarareddy K. Synthesis and spectral characterization of new bis(2-(pyrimidin-2-yl)ethoxy)alkanes and their pharmacological activity. Archiv der Pharmazie. 2012; 345:663–669. [PubMed: 22592977]
41. Rao VK, Babu BH, Babu KR, Srinivasulu D, Raju CN. Ecofriendly Synthesis of Tetrahydropyrimidine Derivatives in Aqueous Medium under Ultrasonic Irradiation. Synthetic Commun. 2012; 42:3368–3376.
42. Rao VK, Reddy SS, Krishna BS, Naidu KRM, Raju CN, Ghosh SK. Synthesis of Schiff's bases in aqueous medium: a green alternative approach with effective mass yield and high reaction rates. Green Chem Lett Rev. 2010; 3:217–223.
43. Halgren TA. Merck molecular force field .1. Basis, form, scope, parameterization, and performance of MMFF94. Journal of computational chemistry. 1996; 17:490–519.
44. Halgren TA, Nachbar RB. Merck molecular force field .4. Conformational energies and geometries for MMFF94. Journal of computational chemistry. 1996; 17:587–615.
45. Lipinski CA, Lombardo F, Dominy BW, Feeney PJ. Experimental and computational approaches to estimate solubility and permeability in drug discovery and development settings. Adv Drug Deliver Rev. 1997; 23:3–25.
46. Lipinski CA, Lombardo F, Dominy BW, Feeney PJ. Experimental and computational approaches to estimate solubility and permeability in drug discovery and development settings. Adv Drug Deliver Rev. 2001; 46:3–26.
47. Valasani KR, Chaney MO, Day VW, Shidu Yan S. Acetylcholinesterase Inhibitors: Structure Based Design, Synthesis, Pharmacophore Modeling and Virtual Screening. Journal of chemical information and modeling. 2013
48. Valasani KR, Hu G, Chaney MO, Yan SS. Structure-based design and synthesis of benzothiazole phosphonate analogues with inhibitors of human ABAD-Abeta for treatment of Alzheimer's disease. Chemical biology & drug design. 2013; 81:238–249. [PubMed: 23039767]

49. Moberg P, Stahl A, Bhushan S, Wright SJ, Eriksson A, Bruce BD, Glaser E. Characterization of a novel zinc metalloprotease involved in degrading targeting peptides in mitochondria and chloroplasts. The Plant journal : for cell and molecular biology. 2003; 36:616–628. [PubMed: 14617063]

50. Stahl A, Moberg P, Ytterberg J, Panfilov O, Brockenhuus Von Lowenhielm H, Nilsson F, Glaser E. Isolation and identification of a novel mitochondrial metalloprotease (PreP) that degrades targeting presequences in plants. The Journal of biological chemistry. 2002; 277:41931–41939. [PubMed: 12138166]

51. Stahl A, Pavlov PF, Szigyarto C, Glaser E. Rapid degradation of the presequence of the f1beta precursor of the ATP synthase inside mitochondria. The Biochemical journal. 2000; 349(Pt 3): 703–707. [PubMed: 10903130]

- We have deigned and synthesized hPreP antagonists for treatment of Alzheimer's Disease.
- Title compounds enhanced hPreP-mediated proteolysis of amyloid beta (Aβ).
- Aβ (1–42), $pF_1\beta$ (2–54) and fluorogenic-substrate V were used as substrates of hPreP.
- **3c** & **4c** showed potent enhancement of hPreP-mediated proteolysis various substrates in vitro.

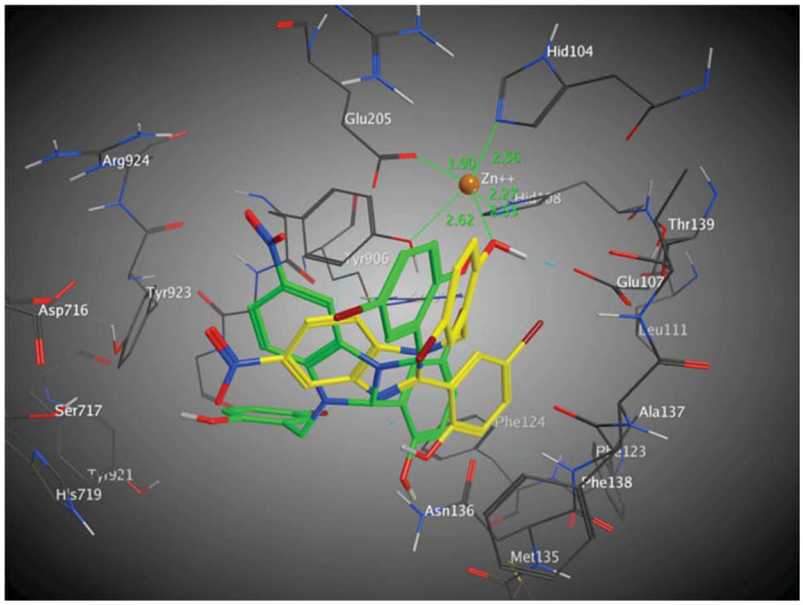

Figure 1.

hPreP binding site for compounds **3c** (yellow) and **4c** (green). Shown are the interacting residues within 5 A° that stabilize the binding of these two compounds. Residues are labeled with residue number. The Zn cation ligand coordinates with residues Try906, Glu205, His104 and His108. Coordination distances range from 1.0 to 2.6 A°. Interestingly, the (2, 5-Bz) group on compound **3c** appears to be involved with this coordination forming a bipyramidal trigonal complex with its OH group. Although the equivalent aromatic hydroxy for compound **4c** is oriented in the same direction, it is further away (3.6 A°) and forms a much weaker bond.

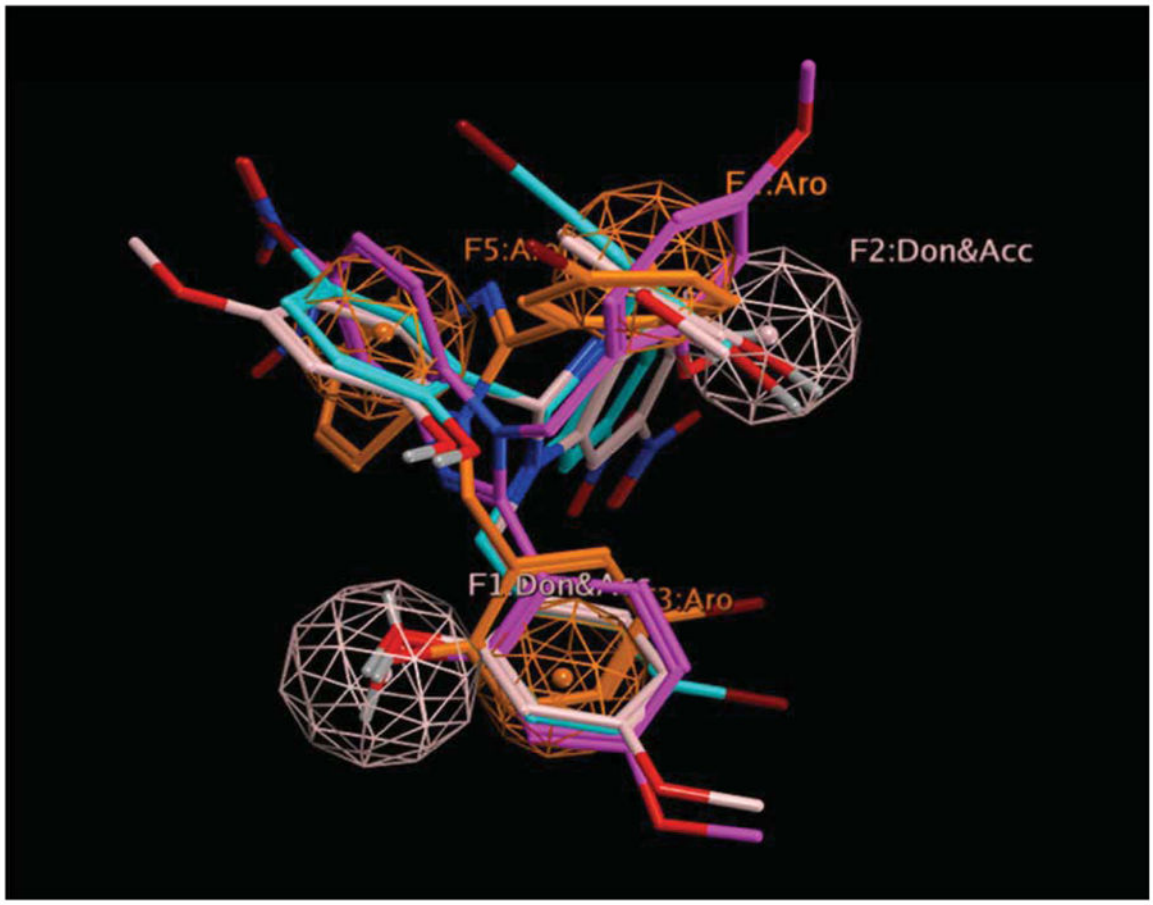

Figure 2.

The predicted active hits for our 5-feature pharmacophore model. Spheres represent the important regions in space for tight ligand binding. The two pink regions show H-bonding, while orange shows 3 regions that characterize aromaticity. The 4 active hits are identified by their “bond stick” colors: **3c** (orange), **3d** (magenta), **4c** (turquoise) and **4d** (white).

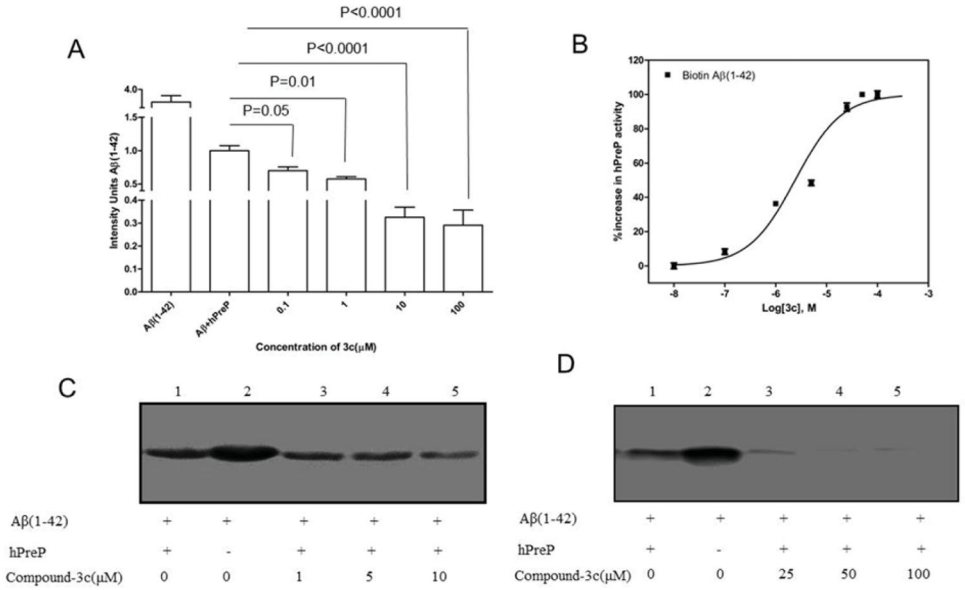

Figure 3.

Effect of compound 3c on Aβ degradation. (A) Densitometry of Aβ immunoreactive bands is shown by analysis using NIH ImageJ software. Determination of proteolytic activity of hPreP showing degradation of biotin-Aβ (1–42), pure hPreP protein was incubated with Aβ (1–42) and various concentrations of compound 3c, which was then subjected to immunoblotting with ExtrAvidin peroxidase conjugated IgG and detection with ECL to reveal immunoreactive biotin Aβ. (B) Measurement of increases in hPreP activity for Aβ (1–42) in the presence of compound 3c at concentrations ranging from 100 to 0.01μM. The panels C and D showed the representative gel images.

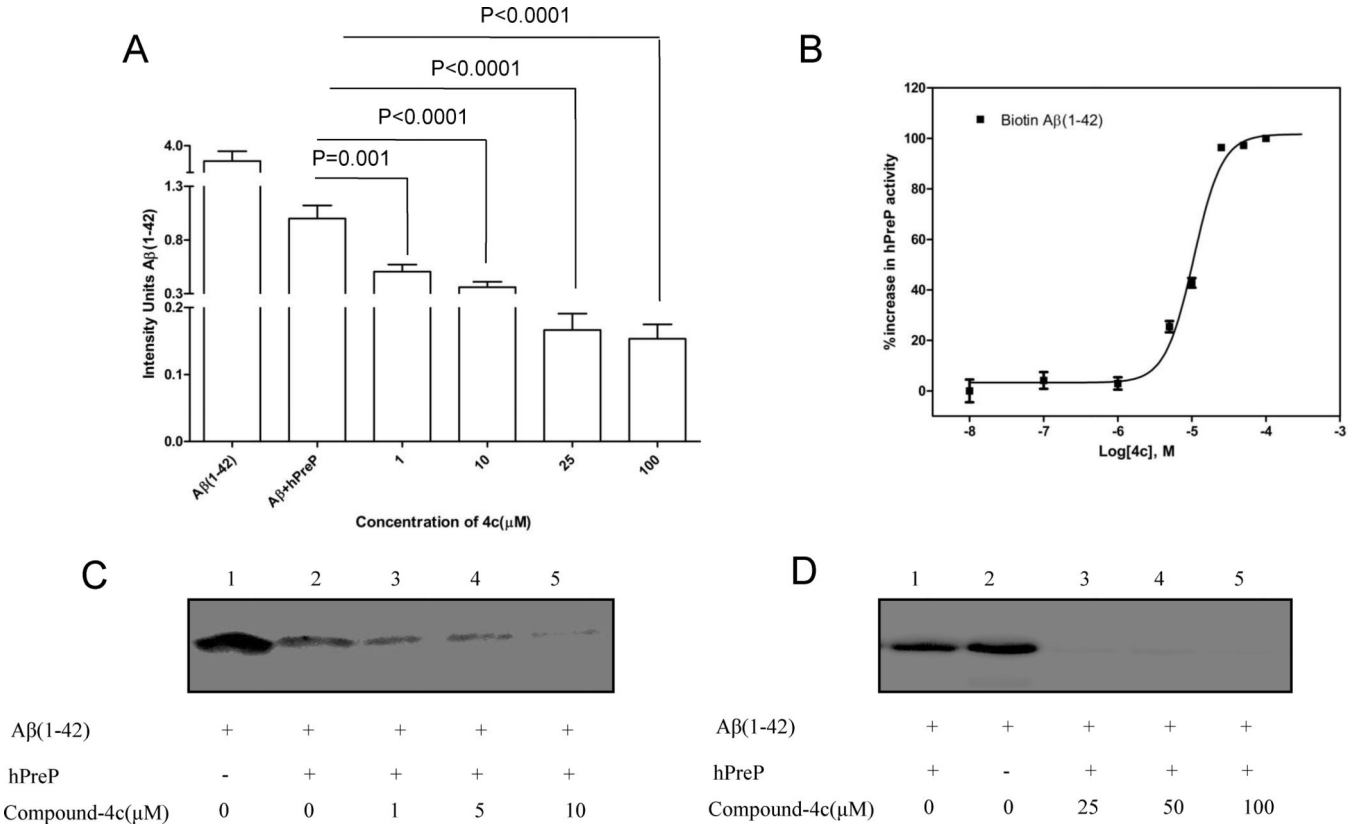

Figure 4.

Effect of compound **4c** on Aβ degradation. (A) Densitometry of Aβ immunoreactive bands is shown using NIH ImageJ software. Determination of proteolytic activity of hPreP showing degradation of biotin-Aβ (1–42), pure hPreP protein was incubated with Aβ (1–42) and various concentrations of compound 4c, which was then subjected to immunoblotting with ExtrAvidin peroxidase conjugated IgG and detection with ECL to reveal immunoreactive biotin Aβ. (B) Measurement of increased hPreP activity for Aβ (1–42) in the presence of compound 4c at concentrations ranging from 100 to 0.01μM. The panel C and D showed the representative gel images.

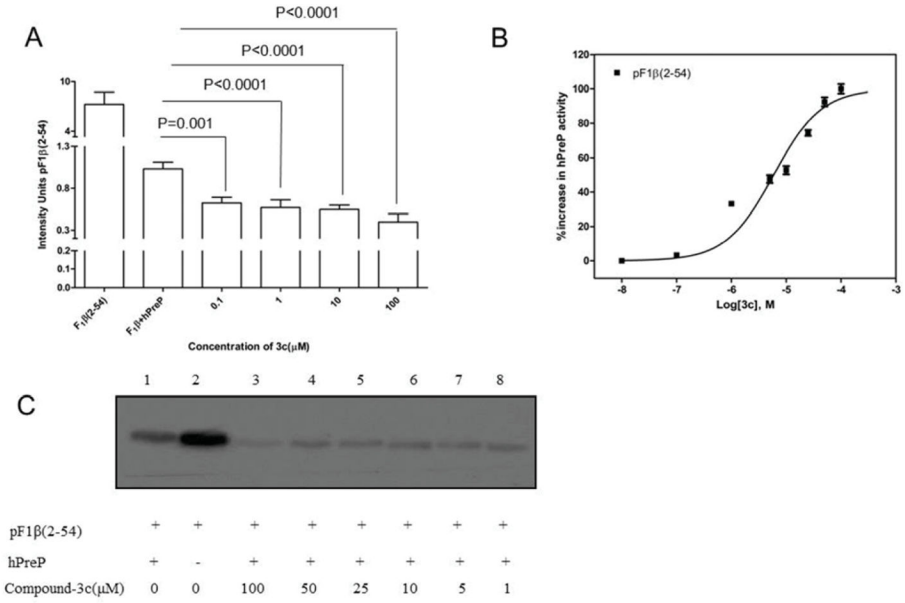

Figure 5.

Effect of compound 3c on pF1β degradation. (A) Densitometry of pF1β immunoreactive bands is shown using NIH ImageJ software. Determination of proteolytic activity of hPreP showing degradation of pF1β, pure hPreP protein was incubated with pF1β and various concentrations of compound 3c, which was then subjected to immunoblotting with antibody to F1β and detection with ECL to reveal immunoreactive biotin Aβ. (B) Measurement of increased hPreP activity for pF1β in the presence of compound 3c at concentrations ranging from 100 to 0.01μM. The panel C demonstrated the representative gel image.

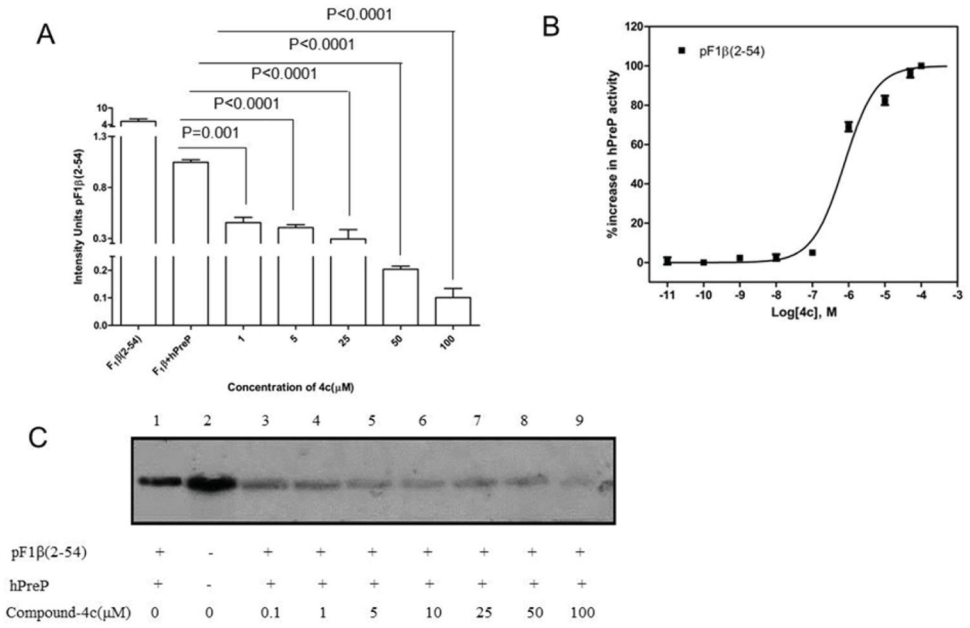

Figure 6.

Effect of compound 4c on pF1β degradation. (A) Densitometry of pF1β immunoreactive bands is shown using NIH ImageJ software. Determination of proteolytic activity of hPreP showing degradation of pF1β, pure hPreP protein was incubated with pF1β and various concentrations of compound 4c, which were then subjected to immunoblotting with antibody to F1β and detection with ECL to reveal immunoreactive biotin Aβ. (B) Measurement of increases in hPreP activity for pF1β in the presence of compound 4c at concentrations ranging from 100 to 0.01μM. The panel C demonstrated the representative gel image.

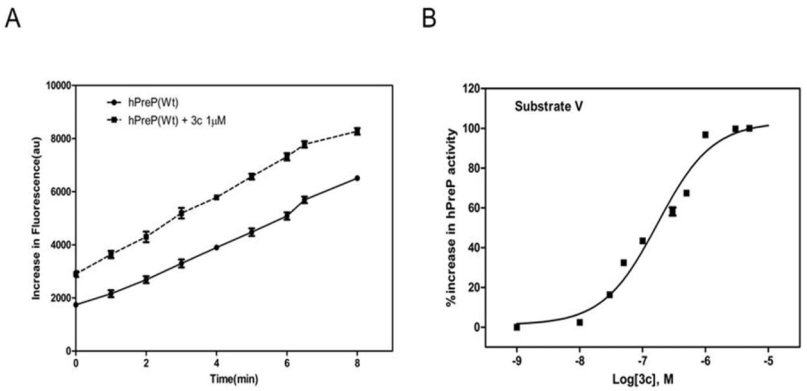

Figure 7.

Kinetics of degradation of fluorogenic Substrate V by hPreP in the presence of compound-3c at 1μM. (A) The change in fluorescence quenching was measured with excitation and emission wavelength set at 320 nm and 405 nm, respectively. (B) Measurement of increases in hPreP activity for Substrate V degradation in the presence of 3c at concentrations ranging from 0.00001 to 5μM.

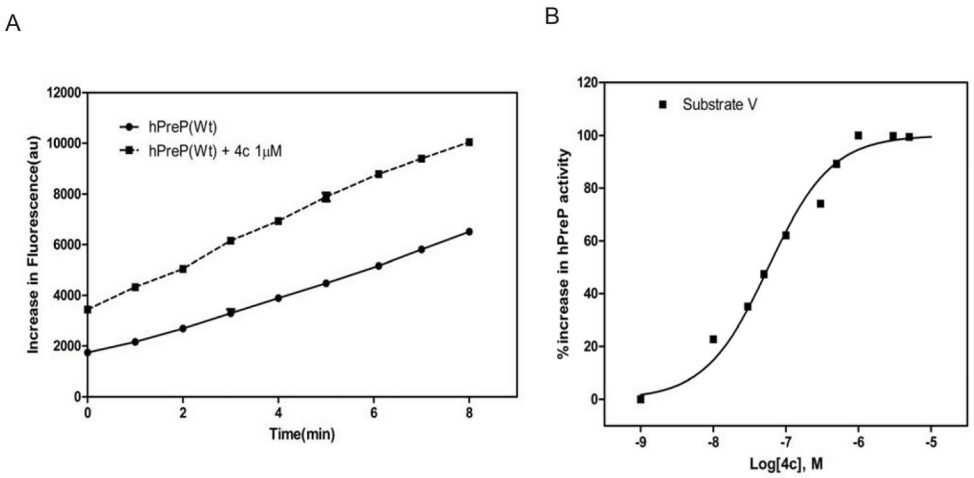

Figure 8.

Kinetics of degradation of the fluorogenic Substrate V by hPreP in the presence of compound-4c at 1μM. (A) The change in fluorescence quenching was measured with excitation and emission wavelength set at 320 nm and 405 nm, respectively. (B) Measurement of increases in hPreP activity for Substrate V degradation in the presence of 4c at concentrations ranging from 0.00001 to 5μM.

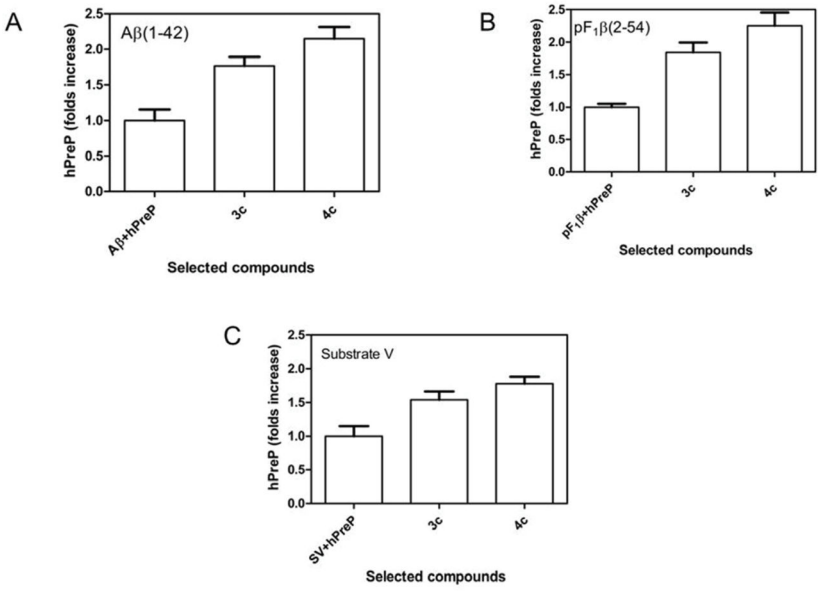

Figure 9.

The change in magnitude of hPreP activity for three substrates. (A) Compound 3c & 4c showed folds increase respectively in the magnitude of hPreP activity for Aβ (1–42). Densitometry of Aβ (1–42) immunoreactive bands is shown. (B) Compound 3c & 4c show folds increase, respectively, in the magnitude of hPreP activity for pF1β (2–54). (C) Compound 3c & 4c show folds increase, respectively, in the magnitude of hPreP activity for substrate V.

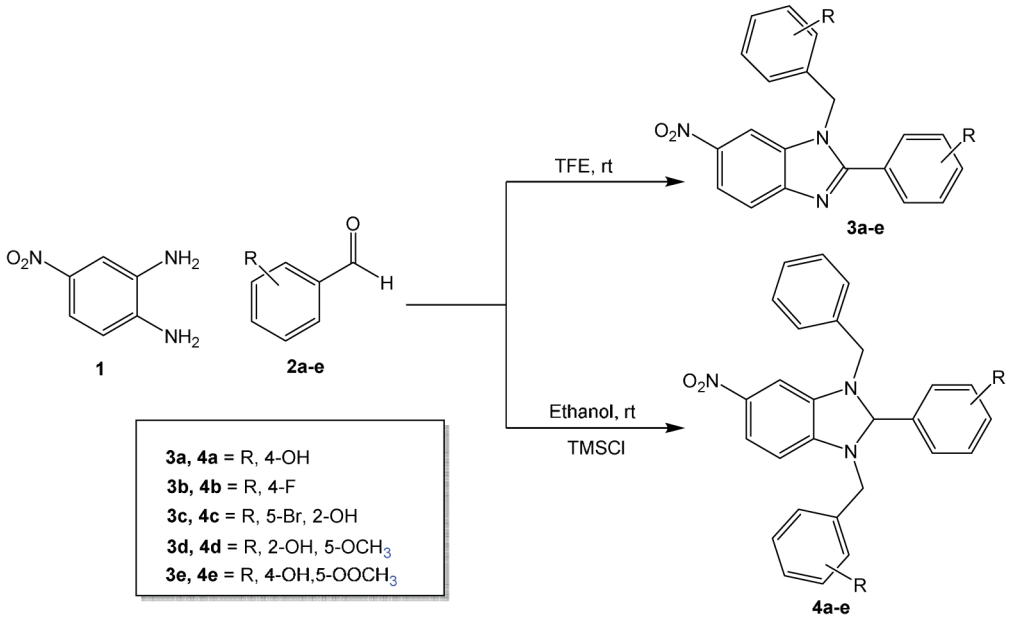

Scheme 1.

Selective synthesis of imidazole scaffold and selected molecular targets of human PreP activators.

Table 1

QSAR descriptors defined for the title compounds.

Ligand	Molecular Weight (Daltans)	Hydrogen Bond Donors	Hydrogen Bond Acceptors	LogP	Molar Refractivity (A^{o3})	Surface area (A^{o2})	Volume (A^{o3})	Solvation energy (K.cal/mol)	Polarizability (A^{o3})	Total energy (K.cal/mol)
3a	361.36	0	1	3.163	28.89	194.836	847.50	−229.942	37.92	48.555
3b	365.34	0	1	3.783	9.777	200.194	315.50	−3.525	51.220	103.523
3c	380.96	1	2	2.464	11.215	255.022	349.63	−190.670	57.103	95.472
3d	421.41	1	4	2.532	11.075	234.676	368.38	−277.640	60.835	141.465
3e	477.43	1	3	2.415	11.819	276.378	382.00	−379.375	63.291	140.796
4a	469.49	3	3	5.992	13.304	235.875	438.13	−11.079	70.166	101.738
4b	465.47	0	0	6.773	12.674	149.987	426.00	−6.174	67.004	101.092
4c	702.90	3	3	6.076	15.588	327.553	507.25	−0.595	81.257	105.810
4d	559.57	3	6	5.965	15.270	290.167	513.38	1.280	81.853	127.623
4e	643.61	3	6	5.92	16.706	374.722	565.88	20.678	89.539	146.564